Revisiting Reconstruction-based AI-generated Image Detection: A Geometric Perspective

Wan Jiang, Jing Yan, Ruixuan Zhang, Xiaojing Chen, Changtao Miao, Zhe Li, Chenhao Lin, Yunfeng Diao, Richang Hong

Abstract

The rise of generative Artificial Intelligence (AI) has made detecting AI-generated images a critical challenge for ensuring authenticity. Existing reconstruction-based methods lack theoretical foundations and on empirical heuristics, limiting interpretability and reliability. In this paper, we introduce the Jacobian-Spectral Lower Bound for reconstruction error from a geometric perspective, showing that real images off the reconstruction manifold exhibit a non-trivial error lower bound, while generated images on the manifold have nearzero error. Furthermore, we reveal the limitations of existing methods that rely on static reconstruction error from a single pass. These methods often fail when some real images exhibit lower error than generated ones. This counterintuitive behavior reduces detection accuracy and requires dataspecific threshold tuning, limiting their applicability in realworld scenarios. To address these challenges, we propose Re-Gap, a training-free method that computes dynamic reconstruction error by leveraging structured editing operations to introduce controlled perturbations. This enables measuring error changes before and after editing, improving detection accuracy by enhancing error separation. Experimental results show that our method outperforms existing baselines, exhibits robustness to common post-processing operations and generalizes effectively across diverse conditions.

1 Introduction

The rapid development of large-scale generative models has dramatically lowered the barrier to synthesizing photorealistic images. While this technological progress fuels creativity and innovation, it also introduces serious challenges related to misinformation, visual deception, and erosion of public trust. These risks are not hypothetical. In the political sphere, researchers have shown that mainstream AI tools can fabricate convincing scenes, such as false images of President Biden being hospitalized or election officials destroying voting machines (Reuters 2024). In the cultural domain, explicit AI-generated images of singer Taylor Swift went viral on social media in early 2024, drawing over 47 million views and raising privacy concerns (News 2024). In another case, a fake image of an "explosion near the Pentagon" spread rapidly in May 2023, briefly triggering public panic and a short market dip before being debunked (Business 2023). Therefore, detecting AI-generated images has become a critical task for ensuring digital and societal integrity.

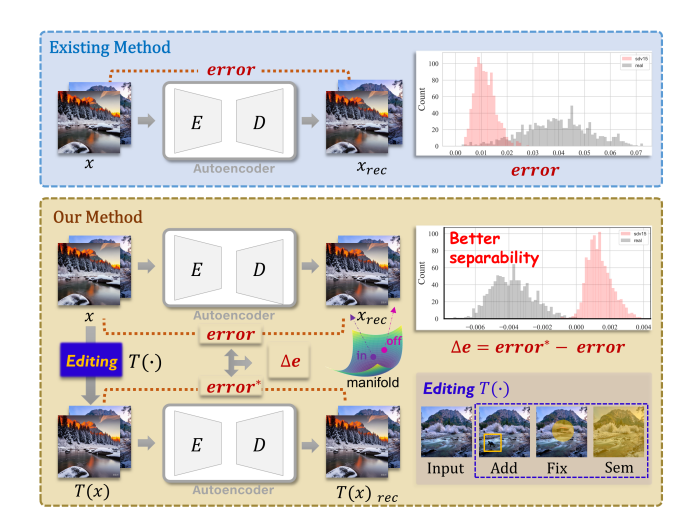


Figure 1: Static vs. Dynamic reconstruction error for detection. Existing methods rely on static reconstruction error with limited separability. Our method applies structured editing to induce dynamic error Δe , enhancing real and generated separability for more effective image detection.

A variety of approaches have been developed to meet the growing demand for reliable generative image detection. Among them, artifact detection (Ba et al. 2024; Huang et al. 2023) and image-text semantic alignment (Yin et al. 2024; Jia et al. 2024) have attracted significant attention. Recent works have explored reconstruction-based approaches (Wang et al. 2023a; Ma et al.; Choi et al. 2024) for detecting generated images, leveraging their flexibility and modelagnostic nature. DIRE (Wang et al. 2023a) estimates reconstruction errors along reverse denoising trajectories, while AERO (Ricker et al.) uses autoencoder-based reconstruction error to distinguish generated images without additional training. As illustrated in Figure 1 (top), these methods are particularly well-suited to open-world scenarios owing to their simplicity and low computational cost. However, despite their empirical success, reconstruction-based detection methods still lack a solid theoretical foundation, which limits their interpretability and generalizability, and hinders robust deployment in complex open-world scenarios.

To fill this gap, we analyze the geometric structure of the decoder's reconstruction manifold and derive the *Jacobian-Spectral Lower Bound for Reconstruction Error*. When the input lies on the reconstruction manifold, the error approaches zero. When it lies off the manifold, its projection induces a residual in the normal space, as illustrated in Figure 2, leading to a non-trivial lower bound governed by the decoder's singular values and the magnitude of the residual. This bound provides support for the observation that real images tend to have larger reconstruction errors, while generated images exhibit errors that asymptotically approach zero.

While this theoretical insight explains the effectiveness of reconstruction-based detection, it also highlights the limitations inherent to static error measures. In practice, when both real and AI-generated images yield similarly low reconstruction errors, such as in cases of simple structures or regular textures, static metrics often fail to ensure reliable separation, leading to false positives or false negatives (Ricker, Lukovnikov, and Fischer 2024). Moreover, most existing methods require training on specific datasets (Zhu et al. 2023; Wang et al. 2023a), which limits their generalizability. Even among training-free approaches that evaluate overall detection performance, there is often a lack of clear criteria for classifying individual images (Choi et al. 2024), which limits their practical applicability.

These limitations underscore the need for detection methods that are both robust and adaptable. We propose **ReGap**, a novel paradigm based on dynamic **Re**construction error that measures the error **Gap** induced by structured edits. Inspired by real-world manipulations, such as object insertion (Add), masked patch regeneration (Fix) and text-guided editing (Sem), these edits introduce meaningful perturbations in latent space along the normal direction of the reconstruction manifold. This approach amplifies the distinction between real and generated images and facilitates reliable and general detection.

Our contributions include both theoretical insights and empirical results, which we summarize as follows:

- To the best of our knowledge, we are the first to establish
 a geometric lower bound on reconstruction error based
 on the singular values of the decoder Jacobian. This result provides a theoretical explanation for the effectiveness of reconstruction error in detecting generated images.
- We propose ReGap, a training-free detection method based on dynamic reconstruction error. It introduces structured latent perturbations and measures resulting error changes to improve the detection. To enhance robustness, we further design a Multi-Edit Max strategy that selects the maximum error among different edit types.
- Extensive experiments support our theoretical analysis and indicate that ReGap performs competitively across diverse datasets and model backbones, while exhibiting robustness to common post-processing operations such as JPEG compression and image cropping.

2 Related Work

Reconstruction-Based Detection of Generated Images.

Reconstruction-based detection emerges as a popular strategy for identifying AI-generated images, particularly in the context of diffusion models. These methods rely on the observation that real and generated images exhibit different behaviors under the reconstruction pipeline. DIRE (Wang et al. 2023a) is an early work that introduces reconstruction error as a signal for diffusion model detection, showing that real and generated images exhibit different reconstruction behaviors. Building on this idea, SeDID (Ma et al.) computes multi-step reconstruction errors to improve discriminative performance. LaRE² (Luo et al. 2024a) further enhances detection accuracy through an error-guided feature refinement module. AERO (Ricker, Lukovnikov, and Fischer 2024) proposes a training-free strategy using the autoencoder of latent diffusion models, and demonstrates competitive results using LPIPS as a perceptual similarity metric. Additionally, HFI (Choi et al. 2024) explores high-frequency sensitivity in autoencoder reconstructions, revealing that frequency can effectively expose distributional discrepancies. Unlike existing methods that rely on static reconstruction errors without theoretical support, we focus on reconstruction dynamics under controlled perturbations. Structured edits amplify latent asymmetries, providing a theoretically grounded signal for detecting generated images.

Latent Space Geometry and Jacobian Analysis. The geometry of latent space fundamentally shapes the behavior of generative models. Prior studies on VAEs and GANs have shown that latent structure affects interpolation smoothness, generation fidelity, and reconstruction accuracy (Arvanitidis, Hansen, and Hauberg 2018; Choi et al. 2025). Decoder sensitivity to latent perturbations is often analyzed through its Jacobian matrix (Sokolić et al. 2017; Hoffman, Roberts, and Yaida 2019). For Latent Diffusion Models (LDMs), recent work has focused mainly on training objectives and generation quality, leaving their reconstruction behavior less understood. AERO (Ricker, Lukovnikov, and Fischer 2024) reported that generated images exhibit much lower reconstruction errors than real images, yet this phenomenon lacks theoretical support. Thus, we leverage the singular value spectra of decoder Jacobians in LDMs to derive a theoretical lower bound on reconstruction error, providing a principled explanation for the gap between real and generated images.

Editing Techniques in Generative Models. Structure editing using diffusion models has emerged as a powerful tool for controllable image manipulation. Recent works like InstructPix2Pix (Brooks, Holynski, and Efros 2023) and Prompt-to-Prompt (Hertz et al. 2023) enable text-guided modifications, while operations like object insertion (Add) and masked patch regeneration (Fix) are widely supported by modern generative models (Tewel et al. 2025; Batifol et al. 2025) and commercial platforms, such as Doubao and Baidu. Existing work that focuses on editing quality, whereas we treat editing as a structured perturbation to reveal latent sensitivity differences between real and generated images. This "editing-as-probing" concept is novel in the context of generative image detection.

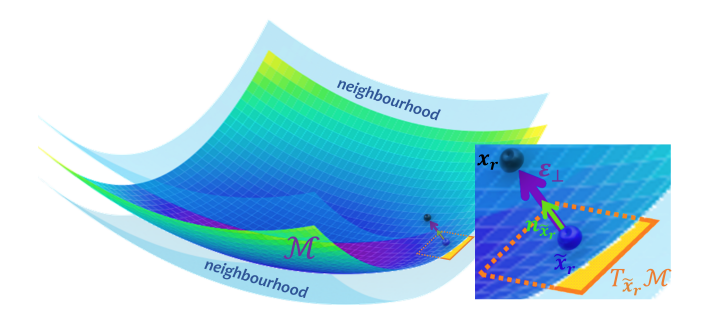


Figure 2: Geometric interpretation of off-manifold projection. An off-manifold point x_r is projected onto the data manifold at \tilde{x}_r . The residual ε_\perp lies along the normal vector $n_{\tilde{x}_r}$, orthogonal to the local tangent space $T_{x_g}\mathcal{M}$, and induces a lower-bounded reconstruction error based on the decoder Jacobian.

3 Method

3.1 Preliminary

Notation. Let the image space be $\mathbb{R}^{H \times W \times 3}$, where H and W denote height and width. We define a pair of continuously differentiable (\mathcal{C}^1) maps:

$$E: \mathbb{R}^{H \times W \times 3} \longrightarrow \mathbb{R}^d, \ D: \mathbb{R}^d \longrightarrow \mathbb{R}^{H \times W \times 3}, \quad (1)$$

where E and D denote the encoder and decoder, and d is the latent space dimension.

Given a latent prior p_z , the reconstruction data manifold generated by the decoder is:

$$\mathcal{M} = \left\{ D(z) \mid z \sim p_z \right\} \subset \mathbb{R}^{H \times W \times 3}. \tag{2}$$

For clarity, all symbols and notations used in this work are summarized in Table 1.

Assumptions. (A1) The encoder E and decoder D are trained such that $E \circ D = \operatorname{id}$ on \mathcal{M} , that is E(D(z)) = z for all $z \sim p_z$. (A2) The decoder D is non-degenerate, meaning its Jacobian $J_D(z)$ has full column rank on the support of the prior. That is $\operatorname{rank} J_D(z) = d, \ \forall \ z \in \operatorname{supp}(p_z),$ where $[J_D(z)]_{ij} = \partial D_i(z)/\partial z_j$ and $\operatorname{supp}(p_z) := \{z \in \mathbb{R}^d \mid p_z(z) > 0\}$. (A3) The decoder D acts as a local C^1 embedding on an open set containing $\operatorname{supp}(p_z)$.

Remark on generality. The assumptions (A1) - (A3) align well with modern generative models. (A1) arises naturally from the reconstruction objectives of VAEs (Kingma and Welling 2014) and diffusion models (Rombach et al. 2022a). (A2) holds empirically on the latent space of VAEs, GANs, and diffusion models (Arvanitidis, Hansen, and Hauberg 2018; Syrota et al. 2025). Although decoders are not globally injective, latent collisions rarely occur in the low-noise region (Yaguchi et al.), which justifies the local embedding assumption (A3)¹.

Symbol	Meaning
$\overline{\mathcal{M}}$	Reconstruction manifold $\mathcal{M} = \{D(z) \mid z \in \mathbb{R}^d\}$
\mathcal{U}	Tubular neighbourhood of \mathcal{M}
x_r	Query image, off-manifold \mathcal{M}
\tilde{x}_r	Nearest point of x_r on \mathcal{M} , i.e., $\tilde{x}_r = \mathcal{P}(x_r)$
$T_{\tilde{x}_r}\mathcal{M}$	Tangent space of \mathcal{M} at \tilde{x}_r
$arepsilon_{\perp}$	Normal deviation $\varepsilon_{\perp} = x_r - \tilde{x}_r, \varepsilon_{\perp} \perp T_{\tilde{x}_r} \mathcal{M}$
z^*	Latent code of \tilde{x}_r : $z^* = E(\tilde{x}_r)$
$J_E(x)$	Jacobian of E at x, a $d \times HW3$ matrix
$J_D(z)$	Jacobian of D at z, a $HW3 \times d$ matrix
$\sigma_{\min}(\cdot)$	Minimum singular value
$\sigma_{\max}(\cdot)$	Maximum singular value
κ_D	condition number $\kappa_D = \sigma_{\max}(J_D)/\sigma_{\min}(J_D)$

Table 1: Symbols and notation used throughout the paper

3.2 Jacobian-Spectral Lower Bound for Reconstruction Error

Under mild regularity assumptions (A1)-(A3), we investigate the behavior of reconstruction error in the vicinity of the decoder's reconstruction manifold. Our goal is to establish a theoretical lower bound on the reconstruction error by analyzing the decoder's local geometric properties, specifically through the lens of its Jacobian condition number. In particular, we model the decoder as implicitly defining a manifold $\mathcal M$ in the data space. For inputs near $\mathcal M$, projecting onto the manifold introduces a residual primarily along the normal direction. Since the decoder exhibits limited sensitivity to off-manifold perturbations, this normal residual is expected to dominate the reconstruction error. We visualize this decomposition intuitively in Figure 2.

To formalize this intuition, we first present a lemma that characterizes the local structure of the decoder around \mathcal{M} , thereby laying the foundation for a principled lower bound on reconstruction error.

Lemma 3.1. Let E and D be C^1 maps satisfying $E \circ D = \operatorname{id}$ on the data manifold M. Then there exists an open neighbourhood U such that for any $x_r \in U$, the nearest point on the manifold M is uniquely defined as

$$\tilde{x}_r = \mathcal{P}(x_r) = \underset{x \in \mathcal{M}}{\arg \min} \|x_r - x\|_2, \tag{3}$$

and x_r can be decomposed as

$$x_r = \tilde{x}_r + \varepsilon_\perp, \ \varepsilon_\perp \perp T_{\tilde{x}_r} \mathcal{M},$$
 (4)

where $T_{\tilde{x}_r}\mathcal{M} = \operatorname{Im} J_D(z^*)$, $z^* := E(\tilde{x}_r)$ and $J_D(z^*)$ is the Jacobian of D evaluated at z^* .

Proof. By the tubular neighborhood theorem (see (Lee 2003), Th. 10.19), any point near \mathcal{M} admits a unique projection with a normal residual orthogonal to the tangent space. See Appendix for details.

Building upon this geometric structure, we now derive a reconstruction error lower bound based on the decoder's Jacobian spectrum.

 $^{^1}$ This is the only geometric requirement required, while alternative condition ensuring the existence of a tubular neighbourhood around $\mathcal M$ would also suffice.

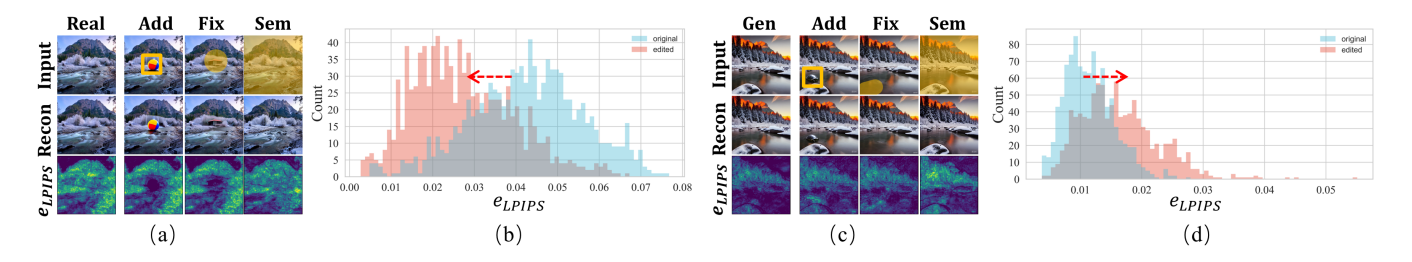


Figure 3: Visualization of dynamic reconstruction error responses for real (a, b) and generated (c, d) images under different structured edits: object insertion (Add), masked patch regeneration (Fix) and text-guided editing (Sem). Panels (a, c) show input images, their reconstructions, and corresponding pixel-wise LPIPS error maps. Panels (b, d) illustrate the distributions of LPIPS reconstruction errors before and after editing. For real images, structured edits induce a leftward shift in the error distribution (decrease; red arrow from blue to red in b), whereas for generated images, the shift is rightward (increase; red arrow in d), thereby enlarging the separation and enhancing detectability. Gray regions in (b) and (d) denote distribution overlap.

Theorem 3.2. Let E and D be C^1 maps satisfying $E \circ D = \operatorname{id}$ on the data manifold M. For any input $x \in \mathbb{R}^{H \times W \times 3}$, let $\tilde{x} \in M$ denote the nearest point on the manifold, and define the normal deviation as $\varepsilon_{\perp} = x - \tilde{x}$. The reconstruction error behaves as follows:

• If $x \in \mathcal{M}$, then $\varepsilon_{\perp} = 0$,

$$||x - D(E(x))||_2 = \mathcal{O}(||\varepsilon_{\perp}||_2^2) \to 0.$$
 (5)

• If $x \notin \mathcal{M}$, then

$$||x - D(E(x))||_2 \ge \sqrt{1 + \kappa_D^{-2}} ||\varepsilon_\perp||_2 + \mathcal{O}(||\varepsilon_\perp||_2^2),$$
 (6)

where $\kappa_D = \sigma_{\max}(J_D)/\sigma_{\min}(J_D)$ is the condition number of the decoder Jacobian evaluated at \tilde{x} .

Proof Outline (full proof in the Appendix). We apply first-order Taylor expansions of E and D:

$$E(x_r) \approx E(\tilde{x}_r) + J_E(\tilde{x}_r)\varepsilon_{\perp},$$
 (7)

$$D(z^* + \Delta z) \approx D(z^*) + J_D(z^*) \Delta z. \tag{8}$$

Combining yields the reconstruction:

$$D(E(x_r)) \approx D(z^*) + J_D(z^*)J_E(\tilde{x}_r)\varepsilon_{\perp}. \tag{9}$$

Thus, the reconstruction error becomes:

$$||x_r - D(E(x_r))||_2 \approx ||\varepsilon_\perp - J_D(z^*)J_E(\tilde{x}_r)\varepsilon_\perp||_2.$$
 (10)

Since ε_{\perp} lies in the normal direction and $J_D(z^*)J_E(\tilde{x}_r)$ maps approximately to the tangent space, this difference is non-zero. Therefore, we obtain the lower bound.

Theorem 3.2 provides strong theoretical support for using reconstruction error to distinguish real from generated images. Specifically, real images lie off the reconstruction manifold and exhibit a non-zero reconstruction error lower bounded by $\sqrt{1+\kappa_D^{-2}}\|\varepsilon_\perp\|_2$, while generated images lie on the manifold with near-zero error. As a direct consequence of this theorem, any perturbation along the normal direction leads to a non-negligible change in reconstruction error, forming the basis for our detection method.

3.3 Dynamic Reconstruction Error Induced by Structured Editing

Despite its widespread use and theoretical support, static reconstruction error suffers from inherent limitations. Specifically, when both real and generated images yield low reconstruction errors in low-texture or symmetric regions, static measures fail to provide reliable separation. Moreover, most training-free methods rely on dataset-specific thresholds to achieve acceptable accuracy, which limits their applicability in real-world, zero-shot scenarios. To address this, we analyze the change in reconstruction error induced by controlled perturbations. Unlike random noise or pixel-level corruption, we apply structured editing operations such as object insertion, region repaint, and semantic editing. These edits follow latent directions defined by the generative model and are designed to simulate realistic manipulations. They introduce localized semantic perturbations while preserving the global semantics of the image. This design ensures that changes in reconstruction error primarily reflect the model's latent sensitivity, rather than a semantic shift in the input.

A key implication of Theorem 3.2 is that any perturbation along the normal direction of the reconstruction manifold induces a non-trivial change in reconstruction error. Structured edits implicitly introduce such semantic deviations, making them an effective mechanism for distinguishing real and generated images. For generated images, these edits often introduce out-of-distribution content, causing them to deviate from the manifold and increasing reconstruction error. In contrast, real images inherently lie off the reconstruction manifold. Structured edits tend to suppress high-error regions by introducing content that conforms more closely to the model's priors, thereby reducing error. This discrepancy is often subtle in static reconstruction but becomes amplified through structured editing, providing a more discriminative signal for detection. Moreover, this asymmetric error response enhances separability, enabling effective detection in training-free settings. Figure 3 illustrates how structured editing affects reconstruction error in real and generated images. Together with our theoretical analysis, these results establish dynamic reconstruction error as a more robust and informative signal for detection.

Method	ADM	BigGAN	GLIDE	Mid	SDv1.4	SDv1.5	VQDM	Wukong	Mean	
Training-based Detection Methods (ACC ↑)										
CNNSpot (Wang et al. 2020)	0.570	0.566	0.571	0.582	0.703	0.702	0.567	0.677	0.617	
Spec (Zhang, Karaman, and Chang 2019)	0.579	0.643	0.654	0.567	0.724	0.723	0.617	0.703	0.651	
F3Net (Qian et al. 2020)	0.665	0.565	0.578	0.551	0.731	0.731	0.621	0.723	0.646	
GramNet (Liu, Qi, and Torr 2020)	0.587	0.612	0.653	0.581	0.728	0.727	0.578	0.713	0.647	
DIRE (Wang et al. 2023b)	0.619	0.567	0.691	0.650	0.737	0.737	0.634	0.743	0.672	
LaRE ² (Luo et al. 2024b)	0.667	0.740	0.813	0.664	0.873	0.871	0.844	0.855	0.791	
	Trair	ning-free Det	ection Met	hods (A	CC↑)					
RIGID (He, Chen, and Ho 2024)	0.514	0.530	0.459	0.941	0.870	0.872	0.522	0.878	0.698	
MIB (Brokman et al. 2025)	0.573	0.776	0.871	0.555	0.620	0.630	0.769	0.654	0.681	
AERO (Ricker et al. 2024)	0.707	0.962	0.957	0.678	0.940	0.933	0.566	0.775	0.814	
$\mathbf{ReGap}_{ au}(\mathbf{ours})$	0.725	0.969	0.959	<u>0.690</u>	$\overline{0.972}$	0.974	0.699	0.902	$\overline{0.861}$	
	Trainii	ng-free Detec	ction Metho	ods (AUI	ROC †)					
RIGID (He, Chen, and Ho 2024)	0.572	0.530	0.539	0.989	0.955	0.954	0.485	0.947	0.746	
MIB (Brokman et al. 2025)	0.681	0.857	0.946	0.628	0.782	0.796	0.874	$\overline{0.793}$	0.795	
AERO (Ricker et al. 2024)	0.839	0.979	0.983	0.850	0.975	0.975	0.708	0.943	0.907	
ReGap(ours)	0.848	0.988	0.984	0.837	0.996	0.998	0.837	0.949	0.930	
Training-free Detection Methods (AP↑)										
RIGID (He, Chen, and Ho 2024)	0.563	0.540	0.342	0.990	0.953	0.951	0.525	0.955	0.727	
MIB (Brokman et al. 2025)	0.654	0.868	0.953	0.609	$\overline{0.723}$	0.734	0.878	0.766	0.773	
AERO (Ricker et al. 2024)	0.839	0.950	0.972	0.827	0.942	0.941	0.684	0.886	0.880	
ReGap(ours)	0.848	0.979	0.979	0.827	0.996	0.998	0.838	0.963	0.928	

Table 2: Comparison of detection methods across diverse generative models. Detection performance is evaluated using Multi-Edit Max with ACC, AUROC and AP. Best in **bold**, second best <u>underlined</u> (applies to all tables).

3.4 ReGap Detection Framework

We formally define our method, ReGap, a training-free detection method that leverages the reconstruction error dynamics induced by structured editing.

Method Overview. Given an input image x, we apply a structured editing operation $T(\cdot)$ to obtain an edited image $\tilde{x} = T(x)$. We then compute the reconstruction errors before and after editing using a pretrained autoencoder $f(\cdot)$:

$$e_{\text{pre}} = d(x, f(x)), \quad e_{\text{post}} = d(\tilde{x}, f(\tilde{x})).$$
 (11)

The dynamic reconstruction error is defined as the absolute difference: $\Delta e = e_{\rm post} - e_{\rm pre}$. The core detection signal is the error difference Δe . An image is detected as generated if $\Delta e > \tau$, and as real otherwise:

$$\Delta e > \tau \Rightarrow \text{generated}, \quad \Delta e \le \tau \Rightarrow \text{real}.$$
 (12)

Following RIGID (He, Chen, and Ho 2024), the threshold τ is selected to ensure that 95% of real images are correctly classified, regardless of the generated images. Figure 1 outlines the overall detection pipeline, highlighting the dynamic reconstruction error response induced by structured edits.

Multi-Edit Max. To improve robustness and generalization, we apply multiple types of edits to each image and compute the **maximum** reconstruction gap across all edits:

$$\Delta e^* = \max_{T \in \mathcal{S}} \{d(T(x), f(T(x))) - d(x, f(x))\}, \quad (13)$$

where S denotes the set of structured editing operations (e.g., Add, Fix, Sem).

4 Experiments

4.1 Experimental setups

Datasets and Metrics. We conduct experiments on the Gen-Image (Zhu et al. 2023) benchmark, where real images are taken from ImageNet (Deng et al. 2009) and generated images are drawn from eight representative generative models: ADM (Dhariwal and Nichol 2021), BigGAN (Brock, Donahue, and Simonyan 2018), GLIDE (Nichol et al. 2022), Midjourney (MidJourney 2022), SD v1.4/1.5 (Rombach et al. 2022b), VQDM (Gu et al. 2022b), and Wukong (Gu et al. 2022a). We follow the work (He, Chen, and Ho 2024; Luo et al. 2024a) and assess detection performance using accuracy (ACC), area under the ROC curve (AUROC) and average precision (AP).

Baselines. We compare representative methods for AI-generated image detection, including both training-based and training-free approaches. The training-based methods include CNNSpot (Wang et al. 2020), Spec (Zhang, Karaman, and Chang 2019), F3Net (Qian et al. 2020), GramNet (Liu, Qi, and Torr 2020), DIRE (Wang et al. 2023b), and LaRE² (Luo et al. 2024b). Following the GenImage protocol, each is trained on one generator and tested on the rest, with results averaged to obtain a single performance score. For training-free methods, AERO (Ricker, Lukovnikov, and Fischer 2024) computes perceptual reconstruction error using LPIPS on the second layer of a pre-trained VGG(LPIPS_{v2}) (Simonyan and Zisserman 2014) network. RIGID (He, Chen, and Ho 2024) exploits the sensi-

tivity of synthetic images to Gaussian noise. MIB (Brokman et al. 2025) performs score-function analysis with a pre-trained diffusion model. These are selected as representative and widely used baselines for detection.

Implementation Details. All experiments are conducted on the GenImage dataset, with images center-cropped and resized to 512×512 pixels. We use Stable Diffusion (SD) v1.5 as the default reconstruction model. Structured editing is performed using the ERNIE-iRAG-Edit model (ERNIE) (Baidu Inc. 2025). We adopt the Multi-Edit Max (M-E Max) strategy to compute dynamic reconstruction error. We use LPIPS_{v2} as the distance metric computed from the second layer of a pre-trained VGG network. We set $\tau = -0.00472$ for ReGap $_{\tau}$. See the supplementary for code and additional details.

4.2 Main results

As shown in Table 2, we evaluate detection methods across eight generative models. For training-based baselines, we adopt a cross-generator validation protocol, where models are trained on one generator and evaluated on the others. Among these methods, LaRE² achieves the highest average accuracy, but its reliance on generator-specific training limits scalability in practice. In contrast, ReGap operates in a zero-shot setting without access to generated data, yet achieves even higher average accuracy. This suggests that dynamic reconstruction responses induced by structured editing enable strong generalization without supervision. We also compare ReGap with training-free methods, including MIB, RIGID, and AERO, which similarly operate without target-generated images. Under the same zero-shot protocol, ReGap outperforms these methods on average while maintaining stable performance across diverse generative models. Although its results are slightly lower on Midjourney and VQDM, this may be attributed to stylized content or lowfrequency structures that reduce editing sensitivity. These results highlight the effectiveness of ReGap in fully trainingfree scenarios. To explain this advantage, we focus on two key design components. First, it introduces structured edits that induce dynamic reconstruction responses, enhancing the separation between real and generated images (Figure 1). Second, it employs a M-E Max strategy that selects the edit with the largest reconstruction gap, improving robustness and ensuring consistent performance across models.

4.3 Sensitivity Analysis

We evaluate the robustness of ReGap under different editing configurations, including edit types, editing models, reconstruction decoders and distance metrics. These experiments assess the method's sensitivity to changes in components. **Effect of Edit Types.** We analyze three representative types

Effect of Edit Types. We analyze three representative types of structured edits: object insertion (Add), masked patch regeneration (Fix) and text-guided editing (Sem). Each operation is applied to images generated by VQDM, SDv1.5 and BigGAN. As shown in Table 3, all editing strategies perform well on SDv1.5 and BigGAN, indicating that ReGap is robust to edit types under high-quality generative models. In contrast, VQDM shows more variation across edit types,

	VQDM			S	SDv1.5	5	BigGAN		
Edit type	ACC	AUC	AP	ACC	AUC	AP	ACC	AUC	AP
Add Fix Sem	<u>68.6</u>	<u>81.7</u>	<u>82.3</u>	97.3	99.9	99.9	94.8	98.4 98.2 98.3	96.8
M-E Max M-E Mean M-E Min	62.7	78.9	79.3	97.5	99.9	99.9	<u>96.5</u>	99.1	98.3

Table 3: Detection performance (%) across different structured edit types. 'AUC' means 'AUROC'.

		BigGAN				
Edit model	ACC	AUROC	AP	ACC	AUROC	AP
ERNIE FLUX.1	0.969 0.944	0.988 0.982	0.,,	0.972 0.896	0.996 0.969	0.996 0.949

Table 4: Detection performance across different editing models.

AE	AD	BG	GL	Mid	SD1.4	SD1.5	VQ	WK	Mean
SDv1.5	84.8	97.9	97.9	82.7	99.6	99.8	83.8	96.3	92.8
SDv2.1	83.5	96.7	97.4	81.3	78.0	77.6	81.3	71.8	83.4
Kandinsky	86.7	98.1	98.3	84.7	67.5	67.1	84.2	62.0	81.0
Ensemble	84.6	97.4	97.7	82.7	99.4	99.4	82.4	<u>95.1</u>	92.3

Table 5: Detection performance (AP (%)) under different auto-encoder backbones.

likely due to its lower visual and structural quality. These results suggest that the effectiveness of edit types varies with their perturbation patterns, but ReGap maintains reliable detection across strategies.

Effect of Editing Models. We evaluate how the choice of editing model affects detection performance. We compare two representative editors: ERNIE, a commercial diffusion model optimized for high-fidelity editing, and FLUX.1 (Batifol et al. 2025), a open-source alternative. As shown in Table 4, both editors perform similarly on BigGAN, suggesting that ReGap is generally robust to the choice of editing backbone under stable generative settings. Under SDv1.4, a slight performance gap is observed. While AUROC and AP remain comparable, FLUX.1 shows a modest drop in accuracy. This may reflect differences in editing fidelity, especially under complex distributions. Editors such as ERNIE exhibit stronger performance through better semantic understanding and high-fidelity generation, supported by largescale training and optimization for consistency and semantic control. These capabilities are critical for producing effective perturbations under complex generative distributions.

Effect of Autoencoders. We evaluate the impact of different autoencoders on detection performance by comparing SDv1.5&SDv2.1 (Rombach et al. 2022c), Kandinsky 2.1 (KD2.1) (Razzhigaev et al. 2023) and an Ensemble strategy (Ricker, Lukovnikov, and Fischer 2024) that selects the minimal error for each input. As shown in Table 5, SDv1.5

achieves the highest AP, outperforming both SDv2.1 and KD2.1. While the ensemble yields comparable results, it incurs higher inference cost due to multiple reconstructions. Overall, SDv1.5 offers the best balance of accuracy and efficiency, making it the default choice in our framework. Our method remains robust across autoencoders, maintaining strong performance even with suboptimal choices. This shows that our structured editing strategy remains effective despite reconstruction differences.

Effect of Distance Metrics. While we use LPIPS $_{v2}$ (L $_{V2}$) as the default perceptual distance, we also evaluate ReGap with a range of alternative metrics. This allows us to assess the robustness of ReGap under different choices of reconstruction distance. These metrics include both perceptual and traditional similarity measures. For perceptual metrics, we consider LPIPS variants based on different backbone networks: VGG16 (L_V) (Simonyan and Zisserman 2014), SqueezeNet (L_S) (Iandola et al. 2016) and AlexNet (L_A) (Krizhevsky, Sutskever, and Hinton 2012). For traditional similarity metrics, we evaluate mean squared error (MSE), structural similarity index (SS) (Wang et al. 2004), contrast-aware SSIM (SC) (Sampat et al. 2009), multiscale SSIM (MS) (Wang, Simoncelli, and Bovik 2003), PSNR, and DISTS (DIS) (Ding et al. 2020). As shown in Table 6, ReGap maintains high detection performance across all settings, demonstrating robustness to distance metrics. L_{V2} performs best mean AP overall, while even simpler metrics like PSNR and MSE yield reasonable results. This confirms that ReGap is not overly sensitive to the distance metric and generalizes well.

4.4 Ablation Study

We conduct an ablation study focusing on our default M-E Max strategy, which selects the edit inducing the maximum reconstruction gap among multiple candidates. This strategy aims to amplify the discrepancy between real and generated samples by exploring diverse perturbation directions. As shown in Table 3, M-E Max achieves the best performance on VQDM, outperforming both single-edit baselines and other M-E strategies. While differences are smaller on SDv1.5 and BigGAN, it remains highly competitive. Although this strategy introduces additional editing overhead, ReGap still performs competitively under single-edit setups. These results validate that M-E Max is effective and robust, offering improved detection without sacrificing generality.

4.5 Robustness to Unseen Perturbations

In real-world scenarios, images shared on social media often undergo post-processing like cropping or compression, which can degrade detection performance. To assess robustness under real-world degradation, we follow existing works (Ricker, Lukovnikov, and Fischer 2024; Choi et al. 2024) and simulate two common perturbation types: JPEG compression (quality q) and center cropping (ratio f), followed by resizing. As shown in Figure 4, our method (red curve) consistently outperforms baselines across degradation levels. In the cropping scenario Figure 4 (a), it maintains stable AP as the f decreases from 1.0 to 0.5, with a peak at f=0.8, likely due to enhanced focus on salient regions.

Dist	AD	BG	GL	Mid	SD1.4	SD1.5	VQ	WK	Mean
L_{V}	78.1	88.0	94.8	84.7	99.6	<u>99.7</u>	77.2	97.9	90.0
L_{V2}	84.8	97.9	97.9	82.7	99.6	99.8	83.8	96.3	92.8
L_{A}	75.3	82.5	94.9	82.2	96.2	96.1	58.0	94.6	85.0
L_S	73.3	81.0	92.4	84.5	98.9	98.9	50.3	94.6	86.0
DIS	62.1	69.4	80.2	68.4	93.1	92.5	43.8	91.1	75.1
MSE	80.6	96.2	96.5	74.8	96.2	96.2	68.0	94.8	87.9
SC	82.2	96.4	96.0	74.1	96.5	96.5	71.8	92.3	88.2
SS	83.9	96.2	96.0	72.8	94.6	94.5	75.3	91.3	88.1
PSNR	79.8	93.9	94.5	63.2	82.2	82.5	69.4	71.1	79.6
MS	78.7	91.9	92.0	66.9	81.5	81.9	70.9	71.9	79.5

Table 6: Detection performance (AP (%)) across distance functions.

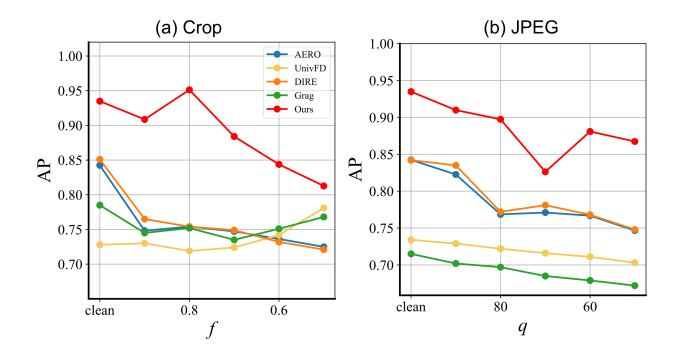


Figure 4: Detection robustness under real-world degradations. (a) AP under different crop ratios f. (b) AP under varying JPEG compression quality q.

In the JPEG compression scenario shown in Figure 4 (b), while other methods degrade significantly with reduced image quality, our method exhibits only a slight drop in AP. Interestingly, a local dip occurs at q=70, which may result from compression artifacts interfering with the editing-based perturbations, but performance quickly recovers at 60, indicating robustness to signal-level distortions. These results confirm that ReGap not only achieves state-of-theart performance under clean conditions but also generalizes well to practical deployment settings where post-processed images are common.

5 Conclusion

In this paper, we introduce a Jacobian-Spectral Lower Bound that provides the first theoretical foundation for reconstruction-based detection. Motivated by the limitations of existing methods, we propose ReGap, a training-free framework that leverages dynamic reconstruction error induced by structured editing to detect AI-generated images. Experiments show that ReGap achieves robust, accurate detection across models and perturbations without relying on generated data. We believe our work opens new possibilities for reliable and generalizable detection of AI-generated content. Future work may extend structured editing to other modalities (e.g., video or audio) and integrating it into broader content verification pipelines for real-world use.

References

- Arvanitidis, G.; Hansen, L. K.; and Hauberg, S. 2018. Latent space oddity: On the curvature of deep generative models. In 6th International Conference on Learning Representations, ICLR 2018.
- Ba, Z.; Liu, Q.; Liu, Z.; Wu, S.; Lin, F.; Lu, L.; and Ren, K. 2024. Exposing the deception: Uncovering more forgery clues for deepfake detection. In *Proceedings of the AAAI Conference on Artificial Intelligence*, volume 38, 719–728.
- Baidu Inc. 2025. ERNIE-iRAG-Edit: Baidu's Image Editing Model. https://ai.baidu.com/model/ernie-irag-edit. Accessed: 2025-08-02.
- Batifol, S.; Blattmann, A.; Boesel, F.; Consul, S.; Diagne, C.; Dockhorn, T.; English, J.; English, Z.; Esser, P.; Kulal, S.; et al. 2025. FLUX. 1 Kontext: Flow Matching for In-Context Image Generation and Editing in Latent Space. *arXiv e-prints*, arXiv–2506.
- Brock, A.; Donahue, J.; and Simonyan, K. 2018. Large scale GAN training for high fidelity natural image synthesis. *arXiv preprint arXiv:1809.11096*.
- Brokman, J.; Giloni, A.; Hofman, O.; Vainshtein, R.; Kojima, H.; and Gilboa, G. 2025. Manifold induced biases for zero-shot and few-shot detection of generated images. *arXiv* preprint arXiv:2504.15470.
- Brooks, T.; Holynski, A.; and Efros, A. A. 2023. Instruct-pix2pix: Learning to follow image editing instructions. In *Proceedings of the IEEE/CVF conference on computer vision and pattern recognition*, 18392–18402.
- Business, C. 2023. 'Verified' Twitter accounts share fake image of 'explosion' near Pentagon, causing confusion. https://edition.cnn.com/2023/05/22/tech/twitter-fake-image-pentagon-explosion. Accessed: 2025-06-23.
- Choi, J.; Hwang, G.; Cho, H.; and Kang, M. 2025. Analyzing the latent space of GAN through local dimension estimation for disentanglement evaluation. *Pattern Recognition*, 157: 110914.
- Choi, S.; Park, S.; Lee, J.; Kim, S.; Choi, S. J.; and Lee, M. 2024. HFI: A unified framework for training-free detection and implicit watermarking of latent diffusion model generated images. *arXiv* preprint arXiv:2412.20704.
- Deng, J.; Dong, W.; Socher, R.; Li, L.-J.; Li, K.; and Fei-Fei, L. 2009. Imagenet: A large-scale hierarchical image database. In 2009 IEEE conference on computer vision and pattern recognition, 248–255. Ieee.
- Dhariwal, P.; and Nichol, A. 2021. Diffusion models beat gans on image synthesis. *Advances in neural information processing systems*, 34: 8780–8794.
- Ding, K.; Ma, K.; Wang, S.; and Simoncelli, E. P. 2020. Image quality assessment: Unifying structure and texture similarity. *IEEE transactions on pattern analysis and machine intelligence*, 44(5): 2567–2581.
- Gu, J.; Meng, X.; Lu, G.; Hou, L.; Niu, M.; Liang, X.; Yao, L.; Huang, R.; Zhang, W.; Jiang, X.; Xu, C.; and Xu, H. 2022a. Wukong: A 100 Million Large-scale Chinese Crossmodal Pre-training Benchmark. In Advances in Neural Information Processing Systems, Datasets and Benchmarks Track.

- Gu, S.; Chen, D.; Bao, J.; Wen, F.; Zhang, B.; Chen, D.; Yuan, L.; and Guo, B. 2022b. Vector Quantized Diffusion Model for Text-to-Image Synthesis.
- He, Z.; Chen, P.-Y.; and Ho, T.-Y. 2024. Rigid: A training-free and model-agnostic framework for robust ai-generated image detection. *arXiv preprint arXiv:2405.20112*.
- Hertz, A.; Mokady, R.; Tenenbaum, J.; Aberman, K.; Pritch, Y.; and Cohen-Or, D. 2023. Prompt-to-Prompt Image Editing with Cross-Attention Control. In *ICLR*.
- Hoffman, J.; Roberts, D. A.; and Yaida, S. 2019. Robust learning with jacobian regularization. *arXiv preprint arXiv:1908.02729*.
- Huang, B.; Wang, Z.; Yang, J.; Ai, J.; Zou, Q.; Wang, Q.; and Ye, D. 2023. Implicit identity driven deepfake face swapping detection. In *Proceedings of the IEEE/CVF conference on computer vision and pattern recognition*, 4490–4499.
- Iandola, F. N.; Han, S.; Moskewicz, M. W.; Ashraf, K.; Dally, W. J.; and Keutzer, K. 2016. SqueezeNet: AlexNet-level accuracy with 50x fewer parameters and; 0.5 MB model size. *arXiv preprint arXiv:1602.07360*.
- Jia, S.; Lyu, R.; Zhao, K.; Chen, Y.; Yan, Z.; Ju, Y.; Hu, C.; Li, X.; Wu, B.; and Lyu, S. 2024. Can chatgpt detect deepfakes? a study of using multimodal large language models for media forensics. In *Proceedings of the IEEE/CVF Conference on Computer Vision and Pattern Recognition*, 4324–4333.
- Kingma, D. P.; and Welling, M. 2014. Auto-Encoding Variational Bayes. *International Conference on Learning Representations (ICLR)*.
- Krizhevsky, A.; Sutskever, I.; and Hinton, G. E. 2012. Imagenet classification with deep convolutional neural networks. *Advances in neural information processing systems*, 25
- Lee, J. M. 2003. Introduction to Smooth Manifolds. Springer.
- Liu, Z.; Qi, X.; and Torr, P. H. 2020. Global texture enhancement for fake face detection in the wild. In *Proceedings of the IEEE/CVF conference on computer vision and pattern recognition*, 8060–8069.
- Luo, Y.; Du, J.; Yan, K.; and Ding, S. 2024a. LaRE² 2: Latent Reconstruction Error Based Method for Diffusion-Generated Image Detection. In *Proceedings of the IEEE/CVF Conference on Computer Vision and Pattern Recognition*, 17006–17015.
- Luo, Y.; Du, J.; Yan, K.; and Ding, S. 2024b. LaRE²: Latent reconstruction error based method for diffusion-generated image detection. In *Proceedings of the IEEE/CVF Conference on Computer Vision and Pattern Recognition*, 17006–17015.
- Ma, R.; Duan, J.; Kong, F.; Shi, X.; and Xu, K. ???? Exposing the Fake: Effective Diffusion-Generated Images Detection. In *The Second Workshop on New Frontiers in Adversarial Machine Learning*.
- MidJourney. 2022. MidJourney AI Art Generator.
- News, C. 2024. Taylor Swift deepfakes spread online, sparking outrage. https://www.cbsnews.com/news/taylor-

- swift-deepfakes-online-outrage-artificial-intelligence/?utm_source=chatgpt.com. Accessed: 2025-06-23.
- Nichol, A.; Dhariwal, P.; Ramesh, A.; Shyam, P.; Mishkin, P.; McGrew, B.; Sutskever, I.; and Chen, M. 2022. GLIDE: Towards Photorealistic Image Generation and Editing with Text-Guided Diffusion Models.
- Qian, Y.; Yin, G.; Sheng, L.; Chen, Z.; and Shao, J. 2020. Thinking in frequency: Face forgery detection by mining frequency-aware clues. In *European conference on computer vision*, 86–103. Springer.
- Razzhigaev, A.; Shakhmatov, A.; Maltseva, A.; Arkhipkin, V.; Pavlov, I.; Ryabov, I.; Kuts, A.; Panchenko, A.; Kuznetsov, A.; and Dimitrov, D. 2023. Kandinsky: an improved text-to-image synthesis with image prior and latent diffusion. *arXiv preprint arXiv:2310.03502*.
- Reuters. 2024. OpenAI, Microsoft AI tools generate misleading election images, researchers say. https://www.reuters.com/world/us/openai-microsoft-ai-tools-generate-misleading-election-images-researchers-say-2024-03-06/?utm_source=chatgpt.com. Accessed: 2025-06-23.
- Ricker, J.; Lukovnikov, D.; and Fischer, A. 2024. Aeroblade: Training-free detection of latent diffusion images using autoencoder reconstruction error. In *Proceedings of the IEEE/CVF Conference on Computer Vision and Pattern Recognition*, 9130–9140.
- Rombach, R.; Blattmann, A.; Lorenz, D.; Esser, P.; and Ommer, B. 2022a. High-Resolution Image Synthesis with Latent Diffusion Models. In *IEEE/CVF Conference on Computer Vision and Pattern Recognition (CVPR)*, 10684–10695.
- Rombach, R.; Blattmann, A.; Lorenz, D.; Esser, P.; and Ommer, B. 2022b. High-Resolution Image Synthesis with Latent Diffusion Models.
- Rombach, R.; Blattmann, A.; Lorenz, D.; Esser, P.; and Ommer, B. 2022c. High-resolution image synthesis with latent diffusion models. In *Proceedings of the IEEE/CVF conference on computer vision and pattern recognition*, 10684–10695.
- Sampat, M. P.; Wang, Z.; Gupta, S.; Bovik, A. C.; and Markey, M. K. 2009. Complex wavelet structural similarity: A new image similarity index. *IEEE transactions on image processing*, 18(11): 2385–2401.
- Simonyan, K.; and Zisserman, A. 2014. Very deep convolutional networks for large-scale image recognition. *arXiv* preprint arXiv:1409.1556.
- Sokolić, J.; Giryes, R.; Sapiro, G.; and Rodrigues, M. R. 2017. Robust large margin deep neural networks. *IEEE Transactions on Signal Processing*, 65(16): 4265–4280.
- Syrota, S.; Zainchkovskyy, Y.; Xi, J.; Bloem-Reddy, B.; and Hauberg, S. 2025. Identifying metric structures of deep latent variable models. *arXiv preprint arXiv:2502.13757*.
- Tewel, Y.; Gal, R.; Samuel, D.; Atzmon, Y.; Wolf, L.; and Chechik, G. 2025. Add-it: Training-Free Object Insertion in Images With Pretrained Diffusion Models. In *The Thirteenth International Conference on Learning Representations*.

- Wang, S.-Y.; Wang, O.; Zhang, R.; Owens, A.; and Efros, A. A. 2020. CNN-generated images are surprisingly easy to spot... for now. In *Proceedings of the IEEE/CVF conference on computer vision and pattern recognition*, 8695–8704.
- Wang, Z.; Bao, J.; Zhou, W.; Wang, W.; Hu, H.; Chen, H.; and Li, H. 2023a. Dire for diffusion-generated image detection. In *Proceedings of the IEEE/CVF International Conference on Computer Vision*, 22445–22455.
- Wang, Z.; Bao, J.; Zhou, W.; Wang, W.; Hu, H.; Chen, H.; and Li, H. 2023b. Dire for diffusion-generated image detection. In *Proceedings of the IEEE/CVF International Conference on Computer Vision*, 22445–22455.
- Wang, Z.; Bovik, A. C.; Sheikh, H. R.; and Simoncelli, E. P. 2004. Image quality assessment: from error visibility to structural similarity. *IEEE transactions on image processing*, 13(4): 600–612.
- Wang, Z.; Simoncelli, E. P.; and Bovik, A. C. 2003. Multiscale structural similarity for image quality assessment. In *The thrity-seventh asilomar conference on signals, systems & computers*, 2003, volume 2, 1398–1402. Ieee.
- Yaguchi, M.; Sakamoto, K.; Sakamoto, R.; Tanabe, M.; Akagawa, M.; Hayashi, Y.; Suzuki, M.; and Matsuo, Y. ???? The Geometry of Phase Transitions in Diffusion Models: Tubular Neighbourhoods and Singularities.
- Yin, Z.; Wang, J.; Xiao, Y.; Zhao, H.; Li, T.; Zhou, W.; Liu, A.; and Liu, X. 2024. Improving deepfake detection generalization by invariant risk minimization. *IEEE Transactions on Multimedia*, 26: 6785–6798.
- Zhang, X.; Karaman, S.; and Chang, S.-F. 2019. Detecting and simulating artifacts in gan fake images. In 2019 IEEE international workshop on information forensics and security (WIFS), 1–6. IEEE.
- Zhu, M.; Chen, H.; Yan, Q.; Huang, X.; Lin, G.; Li, W.; Tu, Z.; Hu, H.; Hu, J.; and Wang, Y. 2023. Genimage: A million-scale benchmark for detecting ai-generated image. *Advances in Neural Information Processing Systems*, 36: 77771–77782.